OXFORD

Cerebral Cortex, 2023, **33**, 1581–1594
https://doi.org/10.1093/cercor/bhac157
Advance access publication date 19 April 2022
Original Article

Differential gene expression between callosal and ipsilateral projection neurons in the monkey dorsolateral prefrontal and posterior parietal cortices

Dominique Arion[1], John F. Enwright[1], Guillermo Gonzalez-Burgos[1], David A. Lewis[1,2,*]

[1]Department of Psychiatry and Neuroscience, University of Pittsburgh, 3811 O'Hara Street, Pittsburgh, PA 15213, United States,
[2]Department of Neuroscience, University of Pittsburgh, A210 Langley Hall. Pittsburgh, PA 15260, United States
*Corresponding author: Department of Psychiatry and Neuroscience, University of Pittsburgh, Biomedical Science Tower W1654, 3811 O'Hara Street, Pittsburgh, PA 15213-2593, Email: lewisda@upmc.edu

Reciprocal connections between primate dorsolateral prefrontal (DLPFC) and posterior parietal (PPC) cortices, furnished by subsets of layer 3 pyramidal neurons (PNs), contribute to cognitive processes including working memory (WM). A different subset of layer 3 PNs in each region projects to the homotopic region of the contralateral hemisphere. These ipsilateral (IP) and callosal (CP) projections, respectively, appear to be essential for the maintenance and transfer of information during WM. To determine if IP and CP layer 3 PNs in each region differ in their transcriptomes, fluorescent retrograde tracers were used to label IP and CP layer 3 PNs in the DLPFC and PPC from macaque monkeys. Retrogradely-labeled PNs were captured by laser microdissection and analyzed by RNAseq. Numerous differentially expressed genes (DEGs) were detected between IP and CP neurons in each region and the functional pathways containing many of these DEGs were shared across regions. However, DLPFC and PPC displayed opposite patterns of DEG enrichment between IP and CP neurons. Cross-region analyses indicated that the cortical area targeted by IP or CP layer 3 PNs was a strong correlate of their transcriptome profile. These findings suggest that the transcriptomes of layer 3 PNs reflect regional, projection type and target region specificity.

Key words: laser microdissection; pyramidal neurons; retrograde labeling; RNAseq; working memory.

Introduction

Certain cognitive process, such as working memory (WM), attention, and spatial categorization, are mediated by a distributed cortical network in primates. The dorsolateral prefrontal cortex (DLPFC) and the posterior parietal cortex (PPC) are 2 of many areas that contribute to these processes (Goldman-Rakic 1988; Chafee and Goldman-Rakic 1998; Miller and Cohen 2001; Salazar et al. 2012; Crowe et al. 2013), and these cortical regions share multiple characteristics. Both areas are active during spatial WM tasks (Miyashita and Chang 1988; Miller and Desimone 1994; Constantinidis and Steinmetz 1996; Katsuki and Constantinidis 2013), displaying increased metabolic activity (Friedman and Goldman-Rakic 1994) and greater power of gamma band oscillations during the delay period of such tasks (Buschman and Miller 2007; Lundqvist et al. 2020). Also, some excitatory pyramidal neurons (PNs) in layer 3 in both regions are active during the delay period of spatial WM tasks and contribute to bi-directional excitation between the 2 areas (Goldman-Rakic 1995; Chafee and Goldman-Rakic 1998; Hart and Huk 2020).

However, despite their shared involvement in WM processes, each region differentially contributes to certain features of WM, such as capacity of information storage, response accuracy, and resistance to distractor stimuli (Quintana et al. 1989; Miller et al. 1996; Chafee and Goldman-Rakic 2000; Suzuki and Gottlieb 2013; Jacob and Nieder 2014; Hahn et al. 2018; Miller et al. 2018). Moreover, the molecular, morphological, and electrophysiological properties of layer 3 PNs differ between the DLPFC and PPC in macaque monkeys (Gonzalez-Burgos et al. 2019), and within each region, subsets of layer 3 PNs can be distinguished based on the targets of their axonal projections. For example, retrograde tracer experiments suggest that >95% of layer 3 PNs in monkey neocortex furnish a principal axon projection to a single cortical region (Schwartz and Goldman-Rakic 1982, 1984; Andersen et al. 1985). In both the DLPFC and PPC, 2 specific subsets of layer 3 PNs play key roles in WM processes. The first subset furnishes reciprocal connections between the DLPFC and PPC in the same hemisphere; these associational or ipsilateral projections (IP) are critical to the coordinated engagement of both regions in WM tasks (Lundqvist et al. 2020). The second subset of layer 3 PNs in each region, termed callosal, or contralateral projections (CP), provides connections mostly to the homotopic region of the contralateral hemisphere (Petrides and Pandya 1988;

Received: February 17, 2022. **Revised:** March 29, 2022. **Accepted:** March 30, 2022

Cavada and Goldman-Rakic 1989a, 1989b; Barbas and Rempel-Clower 1997; Barbas et al. 2005; Markov et al. 2013), allowing for the interhemispheric transfer of information during WM tasks (Brincat et al. 2021). In addition to differences in their projection targets, IP and CP layer 3 PNs also exhibit multiple differences in dendritic morphology in the macaque DLPFC (Soloway et al. 2002). Thus, although IP and CP layer 3 PNs are distinct neuronal populations in both the DLPFC and PPC of macaque monkeys, the molecular properties that might determine the IP and CP phenotypes are poorly understood and whether these properties are shared or different between DLPFC and PPC have not been examined.

Consequently, in this study we used fluorescent retrograde tracers to selectively label IP and CP layer 3 PNs in both the DLPFC and PPC from post-pubertal macaque monkeys. Laser microdissection was then used to individually capture IP and homotopic CP retrogradely labeled neurons, and pools of each of the 4 types of layer 3 PNs were subjected to RNAseq analyses. We identified numerous differentially expressed genes (DEGs) between IP and CP layer 3 PNs in each region and found that the functional pathways containing many of these DEGs were shared across regions. However, within each pathway many of the DEGs showed the opposite direction of differential expression between regions; that is, genes that were more highly expressed in IP than CP layer 3 PNs in one region were more highly expressed in CP than IP layer 3 PNs in the other region. Furthermore, our cross-region analyses suggested that the cortical area targeted by IP or CP layer 3 PNs might be a stronger correlate of their transcriptome profile than their identity as IP or CP neurons. These findings suggest that the transcriptomes of layer 3 PNs reflect regional, projection type, and target region specificity.

Materials and methods

Animals

Five (3 males; 2 females) post-pubertal (37–40 months of age) Rhesus macaque monkeys (*Macaca mulatta*) were used in these studies. All housing and experimental procedures were conducted in accordance with USDA and National Institutes of Health guidelines and were approved by the University of Pittsburgh Institutional Animal Care and Use Committee.

Surgical procedures

All monkeys were anesthetized with ketamine (25 mg/kg), treated with atropine (0.5 mg/kg) and dexamethasone (0.5 mg/kg), intubated, and placed in a stereotaxic apparatus. Anesthesia was maintained throughout the procedure with 1% isoflurane in 28% O_2/air delivered through the endotracheal tube. Using sterile techniques, the skull was exposed and craniectomies were made over the right DLPFC and left PPC. The dura was resected over each area of interest, and 6–7 injections (0.6 μL per injection site) of inert red (Alexa Fluor 555, Invitrogen-ThermoFisher) or green (Alexa Fluor 488, Invitrogen-Thermofisher, Waltham, MA) fluorescent-labeled cholera toxin subunit B (1% in PBS) were made using a 5-μL Hamilton syringe, 1.2–1.5 mm below the pial surface and spaced ~1 mm apart in the cortical surface. Injections in the right DLPFC were placed dorsal to the caudal principal sulcus and ventral to the superior ramus of the arcuate sulcus and injections in the left PPC were placed immediately ventral to the caudal intraparietal sulcus (Fig. 1). The color of the fluorescent tracer administered in each region was alternated across animals. The exposed areas were covered with Gelfoam and the skin closed. Following the experiment, animals received a systemic antibiotic (cefazolin 25 mg/kg, 2 times daily) and an analgesic (buprenorphine 0.01 mg/kg, 2 times daily) for 4 days. Two weeks after surgery, animals were euthanized as previously described (Gonzalez-Burgos et al. 2019) using methods consistent with the American Veterinary Medical Association Guidelines for the Euthanasia of Animals.

Laser microdissection

For each monkey, coronal cryostat sections (16 μm) from fresh-frozen tissue blocks containing the principal sulcus (left hemisphere) or the intraparietal sulcus (right hemisphere) were cut, mounted onto polyethylene naphthalate membrane (PEN) slides (Leica Microsystems, Buffalo Grove, IL), quickly dried on a heat plate, and stored. Fluorescently-labeled PNs were sampled from the dorsal and ventral banks of the principal sulcus (DLPFC area 46; left hemisphere) or from the lateral bank of the intraparietal sulcus (PPC areas LIP and 7a; right hemisphere) as depicted in Fig. 1. Because most projections between DLPFC and PPC, and most callosal projections from these areas, originate from layer 3 PNs (Andersen et al. 1985; Johnson et al. 1989; Schwartz and Goldman-Rakic 1991; Barbas and Rempel-Clower 1997; Barbas et al. 2005), we sought to collect retrogradely-labeled neurons from layer 3. However, to avoid obscuring fluorescently-labeled, cholera toxin subunit B-positive neurons, sections were not counterstained for Nissl substance; thus, the location of layer 3 in each section was estimated as ~20–50% of the distance between the pial surface and white matter and fluorescently-labeled neurons in this location were laser micro-dissected. From the left DLPFC, we collected CP PNs labeled from the injections in the right DLPFC and IP PNs labeled from the injections in the left PPC. From the right PPC, we collected CP PNs labeled from the injections in the left PPC and IP PNs labeled from the injections in the right DLPFC. For each type of collection in each monkey, 120 individually dissected cells were pooled into one sample for RNAseq. All samples were collected in duplicate. For 2 monkeys (both males), due to a low number of labeled cells, IP PN samples could not be collected from the right PPC.

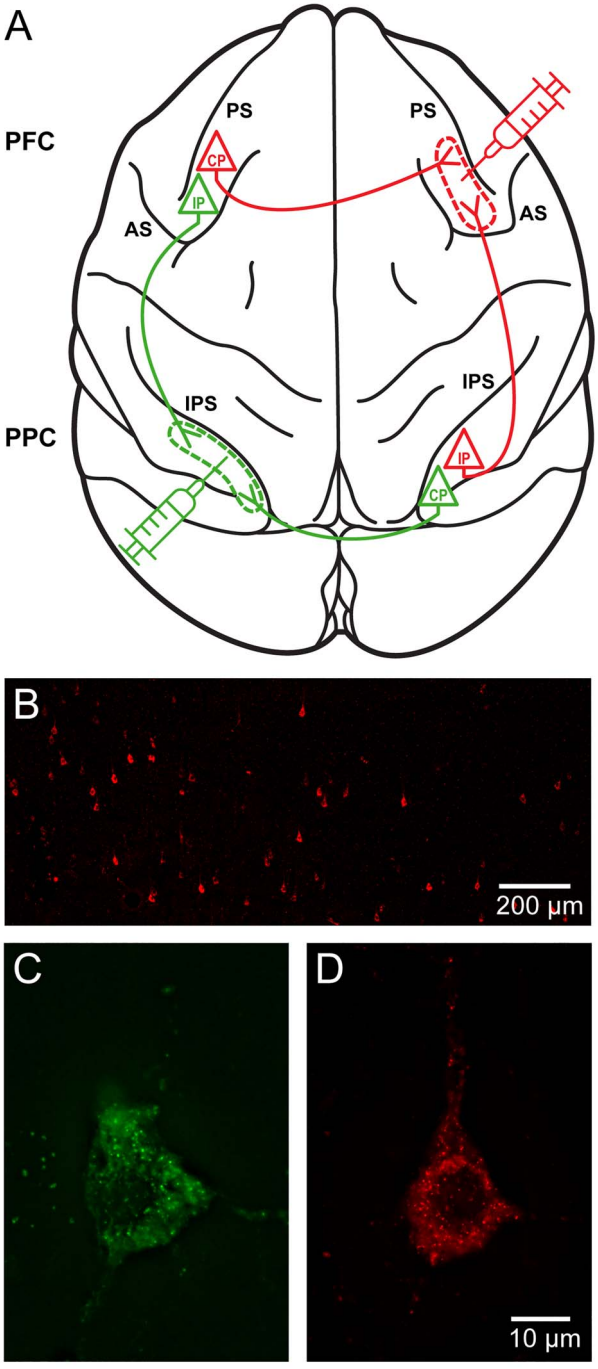

Fig. 1. A) Schematic drawing of the dorsal surface of the macaque brain showing the approximate locations of injections for cholera toxin subunit B, and the locations of sampled retrogradely-labeled layer 3 PNs in DLPFC and PPC. **B**) Low magnification image of layer 3 PNs retrogradely-labeled with red fluorescent cholera toxin subunit B. **C)** Layer 3 PN retrogradely-labeled with green fluorescent cholera toxin B. **D)** Layer 3 PN retrogradely-labeled with red fluorescent cholera toxin subunit B.

RNA isolation, library preparation, and sequencing

Total RNA was extracted from each sample of PNs using the QIAGEN RNeasy Plus Micro kit (QIAGEN, Germantown, MD). Libraries were generated with the Takara SMART-Seq Stranded kit (Takara, Mountain View, CA) using Takara SMARTer RNA Unique Dual Index A and B Kits (Takara, Mountain View, CA) according to the manufacturer's instructions. Expected RNA quality was assessed on samples designated for RNA quality control using an Agilent HS RNA ScreenTape (Agilent: Santa Clara, CA) on an Agilent 2200 TapeStation. Briefly, 7 μL of input RNA was used for each sample with an RNA fragmentation time of 4 min. Each sample was then subjected to 10 cycles of PCR, followed by ribosomal RNA depletion using scZapR, and then a second 10 cycles of PCR. Samples were not pooled at any step in the process. Library assessment and quantification was done using Qubit 1× HS DNA (Life Technologies Corporation, Grand Island, NY) on a Qubit 4 fluorometer and HS NGS Fragment kit (Agilent) on an Agilent 5300 Fragment Analyzer.

Libraries were normalized and pooled by calculating the nM concentration based on the fragment size (base pairs) and the concentration (ng/μL). Prior to sequencing, library pools were quantified by qPCR on the LightCycler 480 (Roche, Indianapolis, IN) using the KAPA qPCR quantification kit (KAPA biosystem, Wilmington, MA). Sequencing was performed using NovaSeq 6000 platform (Illumina, San Diego, CA) to an average of 50 million 101 bp paired-end reads.

Bioinformatic analysis

The paired-end reads were mapped to the reference genome (Mmul 10) using the CLC Genomics software (version 20). Total exon counts for each of 35,395 genes were generated and used for initial quality control analysis. The limma package (Ritchie et al. 2015) in R was used for voom normalization and count per million (CPM) determination for each gene. Initial principal component analysis of the log2 normalized CPM data was performed using the prcomp function in R. Two samples were detected as outliers based on the RNA sequencing metrics. One sample of PPC CP neurons had a library concentration much lower than any other sample (0.01 nM compared with an average of 250 nM) and in one sample of DLPFC IP neurons only 21% of total reads were mapped (compared with an average of 68%). Both samples were excluded from subsequent analyses. Since all samples were originally collected as replicates and these replicates showed >90% correlation with each another, the total counts in each pair of replicate samples (except for the 2 outlier samples) were combined to increase sequencing depth. This resulted in a final set of 18 samples (5 samples each for DLPFC IP and CP layer 3 PNs and for PPC CP layer 3 PNs and 3 samples for PPC IP PNs) with 16 of those being a combination of the 2 replicates (see Supplementary Fig. 1).

To filter out transcripts with very low expression levels without introducing a sex bias, genes with at least 1 CPM in > 8 (the number of samples from female monkeys) of the 18 samples were retained for downstream analysis, resulting in the detection of 12,944 unique genes. These 12,944 genes were used for differential gene expression analysis between regions or cell types within a region. The log2 CPM values along with the precision weights

obtained during voom normalization were used with the limma package (Ritchie et al. 2015). To mitigate the effect of monkey, the Combat function of the Surrogate Variable Analysis package in R (Johnson et al. 2007) was used and sex and library pool/batch were included as covariates in the statistical modeling. Statistical significance for differential expression was determined using the Benjamini–Hochberg procedure with a false discovery rate of 5%. Pathway analysis on >500 canonical pathways was performed with INGENUITY analysis software (IPA) using all filtered genes as background and the tissue filter set to Nervous System. Pathway significance was determined using Fisher's Exact test.

Results

Characteristics of sampled cholera toxin-positive neurons

Because the tissue sections were not counter-stained for Nissl substance, the location of layer 3 had to be estimated based on distance between the pial surface and white matter. In addition, the pattern of cholera toxin fluorescent labeling could not be uniformly used to identify labeled neurons as PNs based on their morphology, although it should be noted that in monkeys < 5% of neurons furnishing axons that project into the white matter are GABAergic and >80% of these neurons are located in deep layers or white matter (Tomioka and Rockland 2007). To verify that the dissected neurons were primarily layer 3 PNs, we made 2 assessments. First, we calculated in each pooled sample the ratio of gene products that are known to be expressed primarily in the superficial (e.g. Cut-like homeobox 2 or CUX2) or deep (e.g. Fez family zinc finger protein 2 or FEZF2) cortical layers (Arion et al. 2007). In all IP and CP samples, CUX2 mRNA levels were at least 18-fold greater than FEZF2 mRNA levels. Second, we calculated the ratio of the excitatory neuron marker SLC17A7 (vesicular glutamate cotransporter 1) to the inhibitory neuron marker SLC32A1 (vesicular GABA transporter). In all IP and CP samples, this ratio was at least 45-fold. Together, these findings confirm that all samples contain primarily layer 3 PNs.

Differential gene expression between CP and IP layer 3 PNs in DLPFC and PPC

In a prior study using microarrays, the gene expression profiles of Nissl-stained layer 3 PNs differed greatly between macaque monkey DLPFC and PPC (Gonzales-Burgos et al. 2019). Therefore, the differential expression analysis of CP and IP layer 3 PNs was performed independently for each region.

In the DLPFC, 682 genes were differentially expressed between CP and IP layer 3 PNs, with 519 (75%) having higher expression in CP layer 3 PNs (Fig. 2A and C, see Supplementary Table 1 for top 20 genes enriched in each PN type). Among these 519 genes, 116 (22%) genes had a >1.5-fold enrichment in CP relative to IP neurons. In contrast, among the 163 genes with higher expression in IP layer 3 PNs, 108 (66%) genes had a >1.5-fold enrichment in IP relative to CP neurons. Pathway analysis of all differentially expressed genes (DEGs) using IPA detected 6 pathways that were significant at a 5% FDR with multiple genes shared among pathways (Table 1). For 2 of these pathways (Protein Kinase A Signaling and Synaptogenesis Signaling) > 70% of the DEGs were enriched in CP neurons.

In the PPC, 337 DEGs were detected between CP and IP layer 3 PNs, with 214 (65%) of these genes having higher expression in IP layer 3 PNs (Fig. 2B and D, see Supplementary Table 2 for top 20 genes enriched in each PN type). Of these 214 genes, 79 (37%) genes had a >1.5-fold enrichment in IP neurons. In contrast, 116 (94%) of the 123 genes with higher expression in CP layer 3 PNs were enriched by >1.5-fold. Pathway analysis of all DEGs using IPA detected 6 pathways that were significant at a 5% FDR (Table 2). For all 6 pathways, over 60% of the DEGs were enriched in IP neurons. Two of these pathways (Synaptogenesis Signaling Pathway and Axonal Guidance Signaling) were also significant in the DLPFC pathway analysis.

In both DLPFC and PPC, the findings of differential gene expression between layer 3 CP and IP neurons were highly consistent across animals. In the DLPFC, 528/682 (77.4%) of the DEGs had the same expression pattern in all 5 animals, and in the PPC, 336/337 (99.7%) of the DEGs had the same expression pattern in the 3 animals in which there were data from both cell types. Examples of the consistency of the findings for select genes are shown in Fig. 2E and F).

Comparison of differential gene expression between CP and IP layer 3 PNs in DLPFC and PPC

The independent analyses of CP and IP neurons in DLPFC and PPC revealed robust differential gene expression between these 2 types of layer 3 PNs in both regions. However, in DLPFC the majority of DEGs (75%) had higher expression in CP neurons, whereas in PPC the majority of DEGs (65%) had higher expression in IP neurons. To explore further this regional difference, we compared the DEGs between cell types within each region. Of the genes that were differentially expressed between CP and IP layer 3 PNs in DLPFC, 93.3% did not differ between CP and IP layer 3 PNs in PPC (Fig. 3A). Similarly, 86.4% of the genes that were differentially expressed between CP and IP neurons in PPC did not differ between CP and IP neurons in DLPFC (Fig. 3B). These comparisons demonstrate that although the same gene pathways differed between CP and IP neurons in both regions, the pattern of differential expression between CP and IP neurons for transcripts within each pathway was region-specific.

Of the 519 genes enriched in CP relative to IP layer 3 PNs in DLPFC, only RORB, PARM1 and COCH (Fig. 3C) were also enriched in CP relative to IP layer 3 PNs in the PPC, but 31 genes showed the opposite pattern of differential expression in the PPC (i.e. higher expression in IP relative to CP layer 3 PNs). In addition, only HS3ST2,

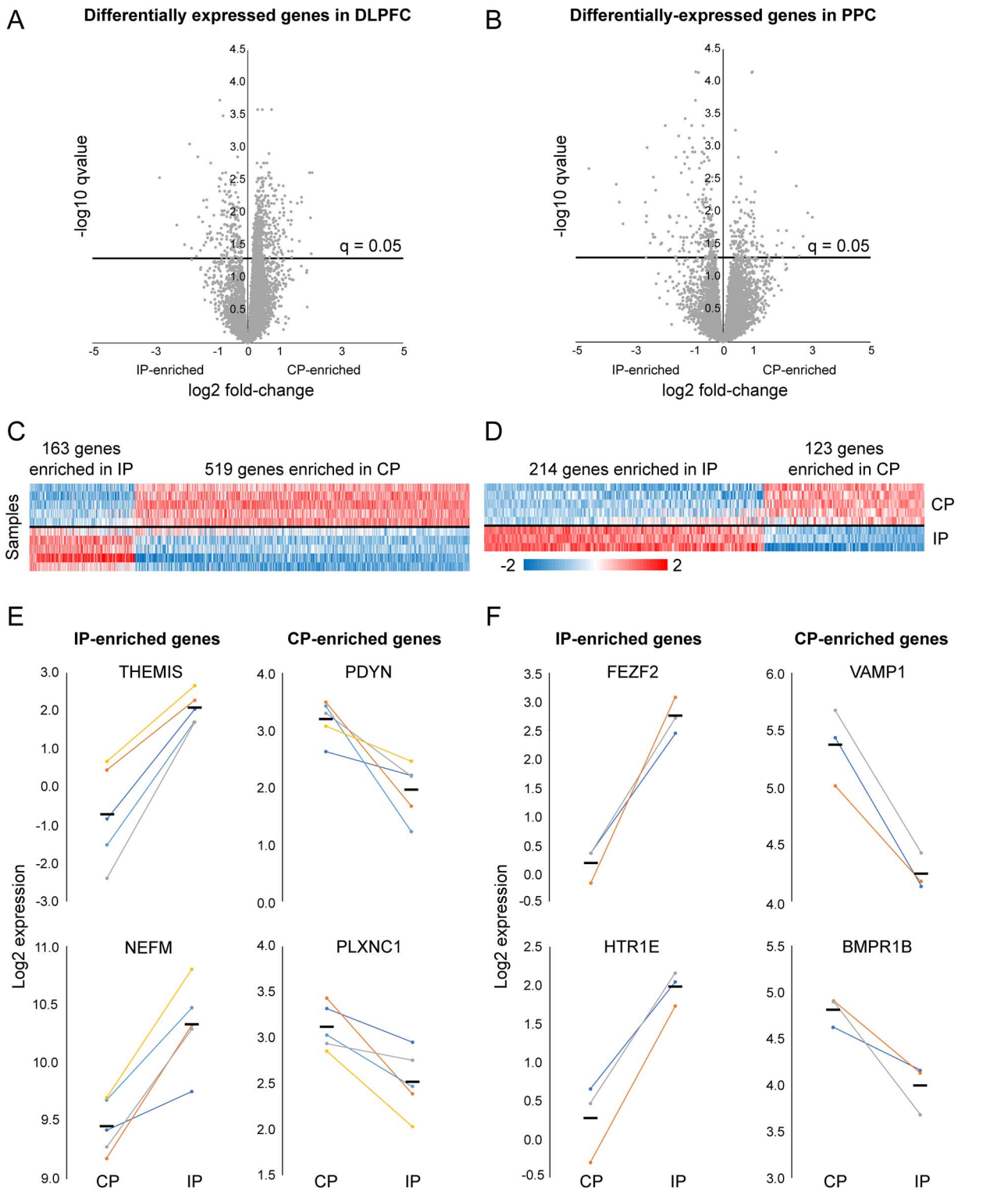

Fig. 2. Differential gene expression between CP and IP layer 3 PNs. **A, B)** Volcano plots of genes expressed in layer 3 PNs in DLPFC and PPC. **C, D)** Heat maps of genes enriched in either CP or IP layer 3 PNs in DLPFC or PPC. The colored scale bar represents *Z*-score normalized gene expression. **E, F)** Examples of enrichment in IP or CP layer 3 PNs from DLPFC or PPC. Colors represent values for individual monkeys. Black bars indicate group means.

INF2, and SEMA3E (Fig. 3C) were enriched in IP relative to CP layer 3 PNs in both regions. Therefore, most DEGs that were enriched in one projection cell type in one region displayed the opposite enrichment pattern between projection cell types in the other region. Moreover, 40 of the 45 genes that were differentially expressed between CP and IP layer 3 PNs in both regions were enriched in CP neurons in one region but in IP neurons in the other region. For example, NEUROD6 expression was significantly enriched by 1.4-fold in CP relative to IP layer 3

Table 1. Gene pathway analysis for IP and CP layer 3 PNs in DLPFC.

Pathway	Genes in pathway	DEGs (%) in pathway	q-Value	DEGs with higher expression in CP PNs	Genes[a]
Synaptogenesis Signaling Pathway	199	34 (17.1%)	2.3E−07	24	CACNA2D1, CAMK2D, CAMK2G, CDH10, CPLX1, CPLX2, CREB1, CTNNB1, DAB1, EFNB3, EPHA4, GRIA2, GRIA4, GRIN2A, GRM5, LIMK1, MAP1B, MRAS, NAPA, NECTIN3, NLGN1, NRXN1, NTRK2, PIK3R1, PRKACB, PRKAR1A, SNAP25, STX1B, SYN2, SYT12, SYT13, SYT16, SYT2, TIAM1
Calcium Signaling	100	20 (20%)	7.8E−06	16	AKAP5, ASPH, ATP2B4, CACNA2D1, CACNA2D2, CAMK2D, CAMK2G, CREB1, GRIA2, GRIA4, GRIN2A, HDAC9, MEF2A, MEF2C, MYH14, PNCK, PRKACB, PRKAR1A, RYR3, SLC8A1
Axonal Guidance Signaling	253	32 (12.6%)	0.001	24	ADAM23, ADAMTS1, ADAMTS15, ADAMTS4, ADAMTS8, BMP2, EFNB3, EPHA4, FZD3, GNB4, GNG4, HHIP, LIMK1, LRRC4C, MRAS, NTNG1, NTRK2, NTRK3, PAK5, PIK3R1, PLCL2, PLXNB2, PLXNC1, PRKACB, PRKAR1A, PRKD1, SEMA3C, SEMA3E, SEMA6D, SEMA7A, UNC5D, WNT7B
Neuropathic Pain Signaling in Dorsal Horn Neurons	69	14 (20.3%)	0.001	12	CAMK2D, CAMK2G, CREB1, ELK1, GRIA2, GRIA4, GRIN2A, GRM5, NTRK2, PIK3R1, PLCL2, PRKACB, PRKAR1A, PRKD1
Cardiac beta-adrenergic Signaling	80	14 (17.5%)	0.02	12	AKAP11, AKAP12, AKAP5, GNB4, GNG4, MPPED2, MRAS, PDE4B, PKIB, PKIG, PPP1CB, PRKACB, PRKAR1A, SLC8A1
Protein Kinase A Signaling	210	26 (12.4%)	0.03	23	AKAP11, AKAP12, AKAP5, CAMK2D, CAMK2G, CREB1, CTNNB1, DUSP6, ELK1, GNB4, GNG4, MPPED2, PDE4B, PLCL2, PPP1CB, PRKACB, PRKAR1A, PRKD1, PTPRA, PTPRF, PTPRG, PTPRR, PTPRT, RYR3, TCF4, YWHAZ

[a]Genes in black are enriched in CP neurons and those in gray are enriched in IP neurons.

Table 2. Gene pathway analysis for IP and CP layer 3 PNs in PPC.

Pathway	Genes in pathway	DEGs (%) in pathway	q-Value	DEGs with higher expression in CP PNs	Genes[a]
CREB Signaling in Neurons	270	25 (9.3%)	1.3E−06	6	ADCYAP1R1, ADGRB2, ADGRG1, ADRA1B, BMPR1B, CACNG3, CNR1, DRD5, FGFR3, GPRC5B, GRIA1, GRIK3, GRIK4, GRM1, HTR1A, MCHR1, PDGFB, PLCE1, PRKCB, PRKCD, PTGER3, RAP2B, RASD1, TACR3, XCR1
Synaptogenesis Signaling Pathway	199	19 (9.6%)	2E−05	6	APOE, CDH11, EFNB3, EIF4EBP2, EPHA6, GRIA1, GRIN3A, GRM1, NRXN2, PRKCD, RAP2B, RASD1, RASGRP1, RASGRP2, SHC3, STX1A, SYN2, SYT17, SYT2
Glutamate Receptor Signaling	40	8 (20%)	5.2E−05	3	GRIA1, GRIK3, GRIK4, GRIN3A, GRM1, SLC17A6, SLC1A2, SLC1A3
Axonal Guidance Signaling	253	20 (7.9%)	0.0003	4	ADAMTS3, ADAMTS8, EFNB3, EPHA6, MMP15, NRP1, PDGFB, PLCE1, PLXNA2, PRKCB, PRKCD, RAP2B, RASD1, ROCK1, RTN4R, SEMA3A, SEMA3E, SLIT1, SLIT3, WNT7A
Breast Cancer Regulation by Stathmin1	241	18 (7.5%)	0.005	3	ADCYAP1R1, ADGRB2, ADGRG1, ADRA1B, CNR1, DRD5, GPRC5B, GRM1, HTR1A, MCHR1, PDGFB, PRKCB, PRKCD, PTGER3, RAP2B, RASD1, TACR3, XCR1
Synaptic Long-Term Depression	100	10 (10%)	0.04	1	CACNG3, GRIA1, GRM1, GUCY1A1, PLCE1, PRKCB, PRKCD, RAP2B, RASD1, RYR3

[a]Genes in black are enriched in CP neurons and those in gray are enriched in IP neurons.

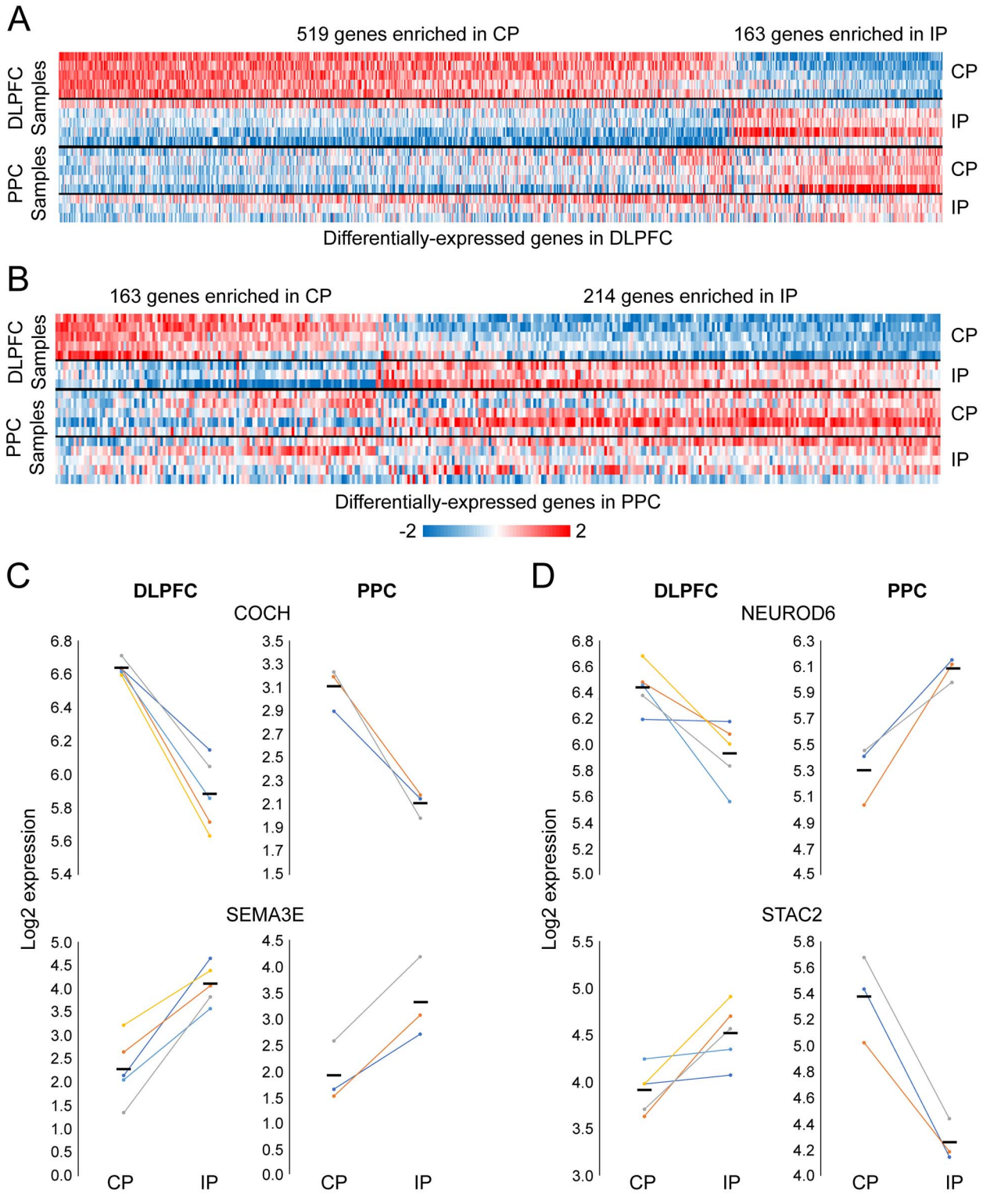

Fig. 3. Comparison of differential gene expression in IP and CP layer 3 PNs between regions. **A)** Heat map of DEGs in DLPFC layer 3 PN subtypes and their expression in PPC layer 3 PN subtypes. **B)** Heat map of DEGs in PPC layer 3 PN subtypes and their expression in DLPFC layer 3 PN subtypes. **C)** Examples of genes showing concordant enrichment patterns in CP and IP layer 3 PNs between regions. **D)** Examples of genes showing the opposite enrichment patterns in CP and IP layer 3 PNs between regions. Colors represent values for individual monkeys. Black bars represent group means.

PNs in DLPFC but was significantly enriched by 1.75-fold in IP relative to CP layer 3 PNs in PPC (Fig. 3D). Conversely, STAC2 expression was significantly enriched by 1.6-fold in IP relative to CP layer 3 PNs in DLPFC but was significantly enriched by 1.78-fold in CP relative to IP layer 3 PNs in PPC (Fig. 3D).

Differential gene expression based on projection target

One possible explanation for genes, such as NEUROD6 and STAC2 (Fig. 3D), with enriched expression in CP neurons in one region but enriched expression in IP neurons in the other region is the presence of a shared projection target that might retrogradely influence gene expression. That is, layer 3 PNs that project to the same target area share certain features of their gene expression profiles, regardless of the regional or hemispheric location of those neurons as suggested by results of prior studies (Sorensen et al. 2015; Fakhry et al. 2015). To test this idea, we compared DLPFC-targeting neurons (i.e. DLPFC CP and PPC IP neurons both of which project to the same DLPFC location) with PPC-targeting neurons (i.e. DLPFC IP and PPC CP neurons both of which project to the same PPC location; see Fig. 1). In an analysis that controlled for the effect of region, 678 genes were differentially expressed between DLPFC- and PPC-targeting layer 3 PNs, with 448 (66%) of those genes having higher expression in DLPFC-targeting PNs (see Supplementary Table 3 for top 20 genes enriched in DLPFC-targeting or PPC-targeting layer 3 PNs). Moreover, 62 genes had a ≥1.5-fold enrichment in DLPFC-targeting PNs, whereas 56 genes had a ≥1.5-fold enriched expression in PPC-targeting PNs (Fig. 4A, B). Pathway analysis of the target-specific DEGs detected 8 pathways, including Synaptogenesis Signaling Pathway, Calcium Signaling, Synaptic Long-Term Depression, and Opioid Signaling Pathway, which have highly overlapping gene sets (Table 3). Principal component analysis (Fig. 4), including all DEGs detected between CP and IP layer 3 PNs in DLPFC (682 DEGs) and PPC (337 DEGs) using the prcomp function in R, clearly separated the samples based on projection target, with target region accounting for 34.9% of the overall variance. Furthermore, the second principal component (26.6% of the variance) separated projection type (CP vs. IP PNs).

Effect of hemisphere on differential gene expression patterns

Due to the nature of the experimental design, all DLPFC neurons were sampled from the left hemisphere and all PPC neurons were sampled from the right hemisphere. To determine if hemisphere influenced the observed patterns of differential gene expression, we compared our findings to the results of our prior study in which Nissl-stained layer 3 PNs were laser microdissected from the DLPFC and PPC of a different cohort of macaque monkeys and subjected to microarray transcriptome profiling (Gonzalez-Burgos et al. 2019). To compare data across the present and prior studies, we first summed data from both IP and CP layer 3 PNs sampled from each brain region in each monkey of the present study and performed differential gene expression analysis between the resulting 5 *left DLPFC* and 5 *right PPC* layer 3 PN samples. Overall, 1,725 genes were differentially expressed between DLPFC and PPC layer 3 PNs, with 1,144 (65%) having higher expression in the DLPFC (Fig. 5A and B). Pathway analysis of the DEGs using IPA detected 2 pathways (Synaptogenesis Signaling Pathway and Glutamate Receptor Signaling) that were significant at a 5% FDR. Of the genes in these 2 pathways, 65% and 80%, respectively, had elevated expression in DLPFC compared with PPC (Table 4). We then compared these findings with our previous microarray analysis of Nissl-stained layer 3 PNs collected from the *right DLPFC* and *left PPC* of a different cohort of 5 Rhesus monkeys (Gonzalez-Burgos et al. 2019). This comparison revealed that the test statistics between the 10,342 genes detected in both studies were positively correlated ($r = 0.44$; $P < 0.0001$). Moreover, of the 1,447 DEGs between DLPFC and PPC detected in the RNA sequencing data reported here that were also detectable in the prior microarray data, 1,214 (83.9%) showed the same direction of regional difference in both studies, even though the 2 studies were conducted in the opposite hemispheres. Thus, these findings support the idea that hemisphere does not confound the regional differences in layer 3 PN gene expression as similar differences between DLPFC and PPC were observed in comparisons of layer 3 PNs from left DLPFC and right PPC (present study) or from right DLPFC and left PPC (Gonzalez-Burgos et al. 2019).

Discussion

In the present study, using RNA sequencing of retrogradely-labeled layer 3 PNs, we found that CP and IP neurons have very different transcriptomes in both DLPFC and PPC of macaque monkeys. Although the functional pathways containing many of these DEGs were shared across regions, within each pathway many of the DEGs showed the opposite direction of differential expression between regions; that is, genes that were more highly expressed in IP than CP layer 3 PNs in one region were more highly expressed in CP than IP layer 3 PNs in the other region. Furthermore, our cross-region analyses suggest that the transcriptomes of layer 3 PNs are also related to the identity of the cortical region innervated by their principal axon projection. In concert, these findings suggest that the transcriptomes of layer 3 PNs reflect regional, projection type and target region specificity.

Technical considerations

In our study design, samples of CP and IP layer 3 PNs that contain cholera toxin conjugates from the left DLPFC and the right PPC were compared. Although hemisphere lateralization is likely to be associated with differential gene expression in certain cortical areas (e.g. those involved in language processing), no hemisphere differences in gene expression were found in 2 studies of the global human transcriptome (Johnson et al. 2009; Hawrylycz et al. 2012). In addition, the DEGs detected between DLPFC and PPC layer 3 PNs in the present study were highly positively correlated with those from a prior transcriptome profiling study using microarrays of layer 3 PNs in

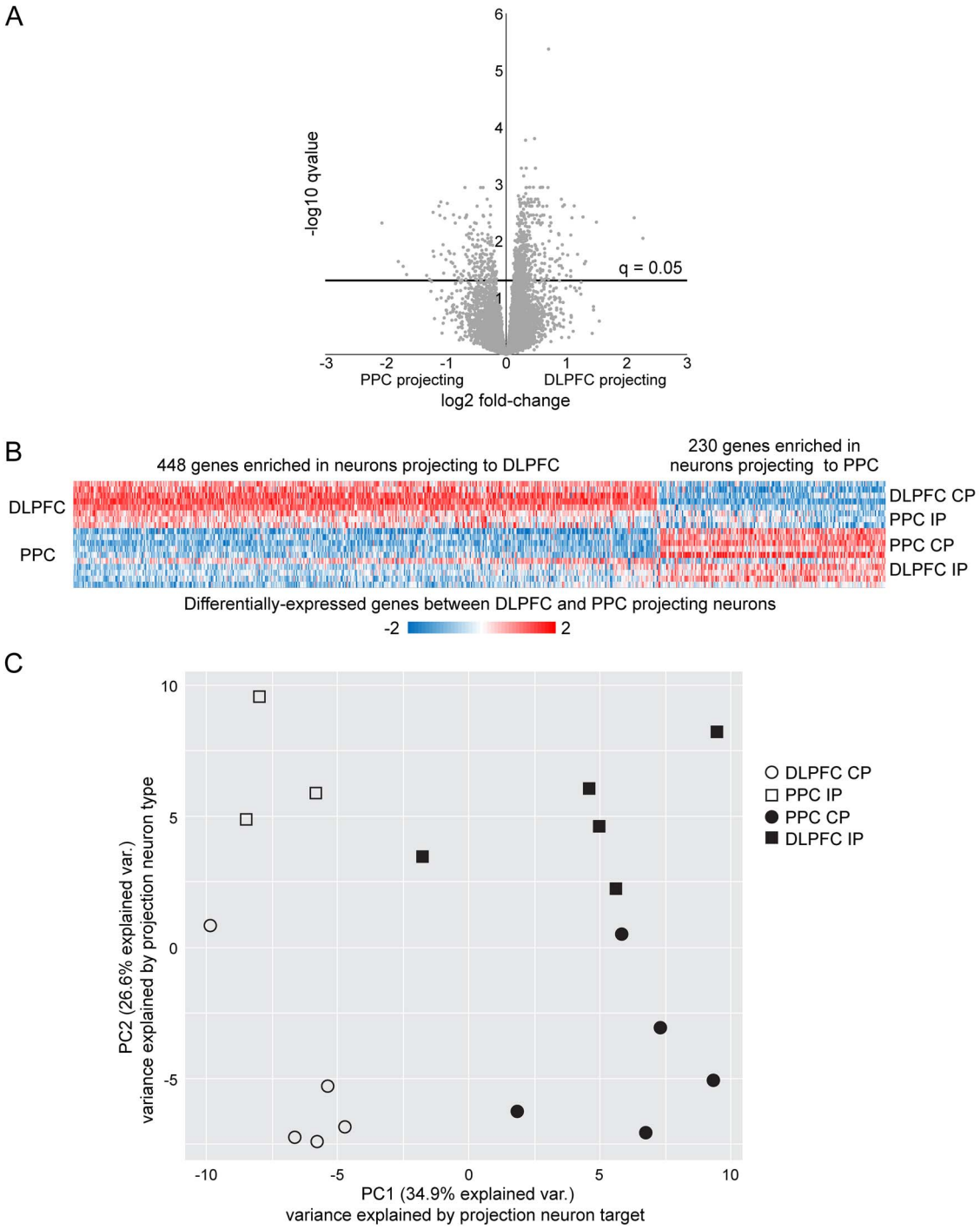

Fig. 4. Differential gene expression between layer 3 PNs projecting to DLPFC or PPC. **A)** Volcano plots of genes expressed in layer 3 PNs projecting to DLPFC or PPC. **B)** Heat map of genes enriched in either DLPFC- or PPC-projecting layer 3 PNs. **C)** Principal component analysis of DEGs detected based on region of origin and projection target. Note that layer 3 PNs clearly segregate based on both on the target of their axon projection (PC1) and the type of projection (PC2).

different hemispheres; importantly, in the latter study, results for selected transcripts were verified by qPCR of DLPFC and PPC layer 3 PNs obtained from the same hemisphere of a different cohort of monkeys (Gonzalez-Burgos et al. 2019). These comparisons suggest that the effect of cortical region on gene expression is much larger than the effect of hemisphere, at least for monkey DLPFC and PPC. Consistent with this interpretation, in a RNAseq analysis comparing laser-microdissected, Nissl-stained layer 3 PNs from the DLPFC and PPC of both hemispheres of the same monkey, we found that region accounted for 33% of the median variance in gene expression and hemisphere accounted for < 2% (data not shown).

Cholera toxin conjugates are made from a recombinant version of the B subunit that is non-toxic to

Table 3. Pathway analysis for genes differentiating DLPFC- and PPC-targeting layer 3 PNs.

Pathway	Genes in pathway	DEGs (%) in pathway	q-Value	DEGs with higher expression in DLPFC-targeting PNs	Genes[a]
Synaptogenesis Signaling Pathway	199	29 (14.6%)	0.004	23	ADCY7, CACNA2D1, CAMK2D, CDH10, CDH11, CPLX1, CPLX2, DNAJC5, EFNB3, GRIA1, GRIA2, GRM1, GRM5, LIMK1, MAPK1, NECTIN1, NECTIN3, PAK1, PIK3R1, PRKCD, RAP2B, RASD1, STX1A, STX1B, SYN2, SYT13, SYT16, SYT17, SYT2
Calcium Signaling	101	19 (18.8%)	0.004	15	AKAP5, ATP2B1, ATP2B4, CACNA1C, CACNA2D1, CACNA2D2, CACNG3, CACNG7, CAMK2D, EP300, GRIA1, GRIA2, HDAC3, MAPK1, PNCK, RAP2B, RCAN2, RYR3, SLC8A1
Synaptic Long -Term Depression	101	17 (16.8%)	0.024	15	CACNA1C, CACNA2D1, CACNA2D2, CACNG3, CACNG7, GRIA1, GRIA2, GRID2, GRM1, GRM5, MAPK1, PLCL2, PRKCD, PRKG1, RAP2B, RASD1, RYR3
Opioid Signaling Pathway	165	23 (13.9%)	0.024	20	ADCY7, CACNA1C, CACNA2D1, CACNA2D2, CACNG3, CACNG7, CAMK2D, EP300, GNB4, KCNJ6, MAPK1, OPRL1, PDE1A, PDE1B, PDE1C, PDYN, PENK, PRKCD, RAP2B, RASD1, RGS7, RYR3, TCF4
Endocannabinoid Neuronal Synapse Pathway	85	15 (17.6%)	0.024	13	ADCY7, CACNA1C, CACNA2D1, CACNA2D2, CACNG3, CACNG7, CNR1, GNB4, GRIA1, GRIA2, GRM1, GRM5, KCNJ6, MAPK1, PLCL2
Role of NFAT in Cardiac Hypertrophy	132	19 (14.4%)	0.045	15	ADCY7, AKAP5, CACNA1C, CACNA2D1, CACNA2D2, CACNG3, CACNG7, CAMK2D, EP300, GNB4, HDAC3, MAPK1, PIK3R1, PLCL2, PRKCD, RAP2B, RASD1, RCAN2, SLC8A1
Amyotrophic Lateral Sclerosis Signaling	75	13 (17.3%)	0.048	9	BIRC3, CACNA1C, CACNA2D1, CACNA2D2, CACNG3, CACNG7, GRIA1, GRIA2, GRID2, NEFL, NEFM, PAK1, PIK3R1
Nitric Oxide Signaling in the Cardiovascular System	67	12 (17.9%)	0.049	10	CACNA1C, CACNA2D1, CACNA2D2, CACNG3, CACNG7, MAPK1, PDE1A, PDE1B, PDE1C, PIK3R1, PRKCD, PRKG1

[a]Genes in black are enriched in DLPFC-targeting neurons and those in gray are enriched in PPC-targeting neurons.

Table 4. Pathway analysis for genes differentiating DLPFC and PPC layer 3 PNs.

Pathway	Genes in pathway	DEGs (%) in pathway	q-Value	DEGs with higher expression in DLPFC	Genes[a]
Synaptogenesis Signaling Pathway	199	55 (27.6%)	2.9E−05	36	ADCY2, ARHGEF7, BAD, CACNA2D1, CAMK2D, CAMK2G, CDH10, CDH11, CDH9, CNTNAP2, CPLX1, CPLX2, EFNB3, EPHA3, EPHA5, EPHA6, EPHB3, GRIA1, GRIA2, GRIA4, GRIN2B, GRM2, GRM5, GRM8, ITPR1, LIMK1, LRRTM2, MAP1B, MRAS, NAP1L1, NECTIN1, NECTIN3, NRXN3, PIK3CG, PIK3R3, PRKACB, PRKCD, RAP1B, RAP2B, RASD1, RASGRP1, RASGRP2, SNCG, STX1B, STXBP5, SYN3, SYNGAP1, SYT16, SYT17, SYT2, SYT9, THBS3, TIAM1, VAMP3, VLDLR
Glutamate Receptor Signaling	40	16 (40%)	0.013	13	GLUL, GNG7, GRIA1, GRIA2, GRIA4, GRID1, GRID2, GRIK2, GRIK4, GRIK5, GRIN2B, GRM2, GRM5, GRM8, HOMER1, SLC17A6

[a]Genes in black are enriched in DLPFC layer 3 PNs and those in gray are enriched in PPC layer 3 PNs.

neurons, as verified previously in multiple studies using these retrograde tracers (Lanciego and Wouterlood 2011; Saleeba et al. 2019). Hence, the presence of these retrograde tracers would not be expected to affect the transcriptome identity of retrogradely-labeled PNs. Consistent with this expectation, the effect of region on gene expression observed in the present study was very similar to that found in our prior study of Nissl-stained layer 3 PNs from monkey DLPFC and PPC (Gonzalez-Burgos et al. 2019). For example, for 2 of the transcripts that were verified by qPCR in the prior study, MET was overexpressed in PPC compared with DLPFC layer 3 PNs by 10.2-fold and

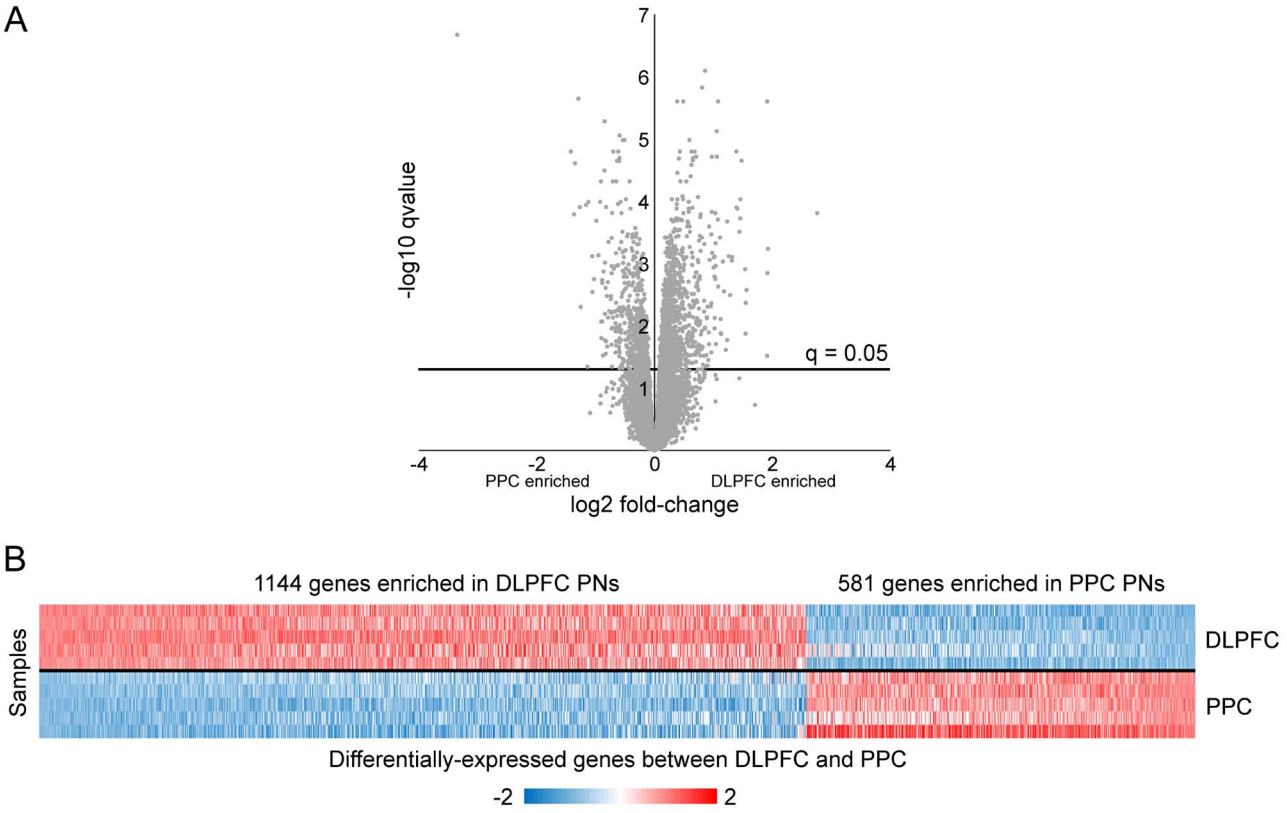

Fig. 5. Differential gene expression between all cholera toxin-labeled layer 3 PNs in DLPFC and PPC: volcano plots of genes expressed in projection neurons from the DLPFC or PPC **A**); Heat map of genes enriched in either DLPFC or PPC layer 3 PNs **B**).

17.5-fold in the current and prior studies, respectively, and CACNA1G was overexpressed in DLPFC compared with PPC layer 3 PNs by 1.9-fold and 1.3-fold, respectively. In concert, these findings suggest that if the presence of cholera toxin B does affect gene expression, the effect is very modest and/or limited to a small number of transcripts.

During microdissection, we noticed that the number of cholera toxin-labeled CP layer 3 PNs in the DLPFC of each monkey was qualitatively greater than the number of labeled IP layer 3 PNs. This observation is consistent with previous retrograde labeling studies, which found that among cortical regions in monkeys, DLPFC has one of the greatest numbers of inter-hemispheric connections (Schwartz et al. 1991; Caminiti et al. 2013), with the number of CP layer 3 PNs exceeding the number of IP layer 3 PNs following injections of retrograde tracers in the ipsilateral PPC and contralateral DLPFC (Schwartz and Goldman-Rakic 1984; Andersen et al. 1985). However, such differences in relative numbers of CP and IP neurons did not confound our study as RNA sequencing was performed on the same number of CP and IP layer 3 PNs in each region. In addition, although the majority of CP PNs project to the homotopic region, some send projections to heterotopic areas (Barbas et al. 2005). However, we cannot comment on the gene expression from this latter subpopulation of CP neurons in comparison with IP neurons as we only collected CP neurons projecting to the homotopic area. Furthermore, in monkey DLPFC layer 3 CP neurons have a larger cell body than IP neurons (Soloway et al. 2002), which could result in the introduction of a bias towards higher transcript levels in CP neurons compared with IP neurons. However, to control for this potential bias, the read count for each transcript in the RNAseq analysis was adjusted for the total number of reads for each sample. Finally, even though we detected numerous DEGs, and the expression differences were highly consistent across individual between monkeys, we cannot exclude the possibility that some DEGs with smaller effect size were not detected due to the sample size of our study.

Distinct transcriptomes of CP and IP layer 3 PNs

In both DLPFC and PPC, CP and IP layer 3 PNs had very different gene expression profiles. This result was not unexpected as previous studies showed that CP and IP PNs in monkeys are separate neuronal populations, even though they are topographically intermingled in layer 3 of both DLPFC and PPC, including within the same cortical columns (Schwartz and Goldman-Rakic 1984; Andersen et al. 1985). Specifically, previous studies reported that, contrary to what is seen in mice (Mitchell and Macklis 2005) $<5\%$ of PNs retrogradely-labeled from ipsilateral and contralateral injection sites were dual-labeled (Schwartz and Goldman-Rakic 1982, 1984; Andersen et al. 1985). Although this study was not designed to determine

the relative number of CP and IP PNs in each region, we rarely encountered dual-labeled PNs in the DLPFC or PPC during cell collection for the present study.

Previous studies reported that total dendritic length, the horizontal extent of the dendritic tree, the complexity of the dendritic arbor and the density of dendritic spines were greater for CP compared with IP neurons in monkey DLPFC (Soloway et al. 2002). Thus, the total number of dendritic spines is greater for CP neurons, suggesting that CP PNs receive more excitatory inputs than IP PNs. Consistent with this difference, we found an enrichment of glutamate receptors transcripts, such as GRIA2, GRIA4, GRIN2A, GRM 5, and GRM7, in CP PNs relative to IP PNs in DLPFC. As the number of spines is lower in PPC compared with DLPFC layer 3 PNs (Elston 2000), the differential expression of glutamate receptors between CP and IP neurons could vary in PPC compared with DLPFC. However, we do not know if the lower complement of dendritic spines in PPC layer 3 PNs is equally present in CP and IP neurons. Nonetheless, we saw an enrichment in glutamate receptors such as GRIA1, GRNIN3A, GRM1, GRIK3, and GRIK4 in IP neurons compared with CP neurons in PPC, which might suggest that, in contrast to the DLPFC, IP neurons in PPC receive more excitatory inputs than CP neurons. Alternatively, given the absence of consistent enrichment differences in transcripts for the obligatory subunits of glutamate receptors, it is possible that differences in glutamate receptor transcript levels may not represent differences in number of glutamate synaptic inputs, but instead differences in the receptor subtypes mediating the synaptic or extrasynaptic response to glutamate.

CP and IP PNs have different developmental timelines that might be associated with their transcriptome differences. For example, in monkeys CP neurons establish their mature interhemispheric connections and projection targets before birth and the number of CP neurons remains stable after the first few months of life (LaMantia and Rakic 1990; Schwartz and Goldman-Rakic 1991). In contrast, IP neuron connections continue to be refined after birth as the elimination of certain associational connections leads to a decrease in the number of retrogradely-labeled IP PNs, especially in layer 3 (Meissirel et al. 1991). Given this difference in the developmental trajectories of anatomical features of layer 3 CP and IP neurons, we predict that the transcriptome of CP layer PNs may be more stable across postnatal development relative to that of IP layer 3 PNs.

Differences in CP and IP layer 3 PN transcriptomes associated with cortical location and target region

The summed data from CP and IP L3 PNs in each region of the present study confirm the results of our prior study of Nissl-stained layer 3 PNs from monkey DLPFC and PPC (Gonzalez-Burgos et al. 2019) that cortical location is associated with differences in the transcriptomes of layer 3 PNs. These findings are also consistent with prior findings that cortical region is a strong determinant of transcriptional identity in macaque monkeys (Bernard et al. 2012).

In addition to this effect of region on gene expression profiles, we also detected numerous DEGs between IP and CP layer 3 PNs in both DLPFC and PPC. Although pathway analyses of these DEGs identified Synaptogenesis and Axonal Guidance pathways as significant in both regions, the expression level for many individual transcripts within each pathway differed between regions. For example, although the 2 larger neurofilament genes, NEFH and NEFM, were more highly expressed by 2.2 and 1.9-fold, respectively, in IP relative to CP layer 3 PNs in DLPFC, expression levels of these transcripts did not differ between IP and CP layer 3 PNs in PPC. These results are consistent with findings from prior studies using the antibody SMI-32, which recognizes a non-phosphorylated epitope of neurofilament proteins (Morrison et al. 1987). In these studies, 42% of IP PNs but only 18% of CP PNs were SMI-32 immunoreactive in monkey DLPFC, whereas in PPC, no differences were found in the proportions of IP PNs (45%) and CP PNs (41%) that were SMI-32-positive (Hof et al. 1995). Furthermore, many of the genes that were differentially expressed between IP and CP neurons in one region showed the opposite enrichment pattern in the other region. For example, NEUROD6, a member of a family of transcription factors regulating neuronal differentiation and axonal navigation, was enriched in CP layer 3 PNs in DLPFC but in IP layer 3 PNs in PPC. Finally, within some gene pathways, the genes that were differentially expressed between CP and IP layer 3 PNs differed between regions. For example, the expression levels for certain GABA (GABRA2, GABRA4, and GABRG2) and glutamate (GRIA2, GRIA4, GRIN2A, GRM5, and GRM7) receptor subunits were greater in CP than in IP layer 3 PNs in DLPFC, whereas in PPC the expression levels of a different set of GABA (GABRA3, GABRA5, and GABRB3–2) and glutamate (GRIA1, GRIN3A, GRM1, GRIK3, and GRIK4) receptor subunit transcripts were greater in IP relative to CP layer 3 PNs.

In concert, these differences suggest that some other factor(s), in addition to region and axonal projection type, is associated with gene expression in layer 3 PNs. Interestingly, our PCA analysis clearly separated samples of layer 3 PNs by the cortical region they targeted (Fig. 4C). The potential influence of target region on gene expression is also supported by our findings that IP PNs in DLPFC and CP PNs in PPC which both project to the PPC have similar patterns of gene expression, as do CP PNs in DLPFC and IP PNs in PPC which both project to the DLPFC (Fig. 4B). For example, previous work has demonstrated the importance of calcium signaling to sustain the firing of DLPFC L3 PNs supporting WM (Arnsten et al. 2021). Interestingly, in our study, the expression of the ryanodine receptor 3 (RYR3), which contributes to

the release of Ca2+ from intracellular stores was significantly greater in PNs projecting to the DLPFC than those projecting to the PPC.

Although differences primates and rodents must be kept in mind, the influence of target region on gene expression is supported by prior findings in the murine somatosensory cortex that (i) axonal projection target was a more important determinant of transcriptional diversity than laminar location or developmental origin (Klingler et al. 2019), and (ii) PNs located in the same cortical layer that express distinct transcripts sent axonal projections to different targets (Sorensen et al. 2015).

Conclusions

In summary, our findings reveal that CP and IP PNs in layer 3 of both DLPFC and PPC possess different cell type-specific transcriptional profiles. These transcriptional profiles appear to reflect differences in region of origin, axonal projection type and the cortical region targeted by the axonal projection. These transcriptional profiles may contribute to the morphological and physiological characteristics of CP and IP neurons in each region, and thus to their differential contributions to WM. Identifying the distinctive molecular characteristics of the neuronal subtypes involved in WM can help inform and interpret studies of alterations in DLPFC and PPC layer 3 PNs in disorders such as schizophrenia where WM deficits are a core component of the disease process.

Supplementary material

Supplementary material can be found at *Cerebral Cortex* online.

Acknowledgments

We thank Kate Gurnsey for assistance in surgical procedure and Kelly Rogers and Mary Brady for excellent technical assistance.

Conflict of interest statement: David A. Lewis currently receives investigator-initiated research support from Merck. All other authors declare no conflict of interest.

Funding

This work was supported by NIH (grant MH051234 to DAL) and Neuronex NSF (grant NSF 2015276 to GGB).

References

Andersen RA, Asanuma C, Cowan WM. Callosal and prefrontal associational projecting cell populations in area 7A of the macaque monkey: a study using retrogradely transported fluorescent dyes. *J Comp Neurol*. 1985:232:443–455.

Arion D, Unger T, Lewis DA, Mirnics K. Molecular markers distinguishing supragranular and infragranular layers in the human prefrontal cortex. *Eur J Neurosci*. 2007:25:1843–1854.

Arnsten AFT, Datta D, Wang M. The genie in the bottle-magnified calcium signaling in dorsolateral prefrontal cortex. *Mol Psychiatry*. 2021:26:3684–3700.

Barbas H, Rempel-Clower N. Cortical structure predicts the pattern of corticocortical connections. *Cereb Cortex*. 1997:7:635–646.

Barbas H, Hilgetag CC, Saha S, Dermon CR, Suski JL. Parallel organization of contralateral and ipsilateral prefrontal cortical projections in the rhesus monkey. *BMC Neurosci*. 2005:6:1–17.

Bernard A, Lubbers LS, Tanis KQ, Luo R, Podtelezhnikov AA, Finney EM, McWhorter MM, Serikawa K, Lemon T, Morgan R, et al. Transcriptional architecture of the primate neocortex. *Neuron*. 2012:73:1083–1099.

Brincat SL, Donoghue JA, Mahnke MK, Komblith S, Lundqvist M, Miller EK. Interhemispheric transfer of working memories. *Neuron*. 2021:109:1–12.

Buschman TJ, Miller EK. Top-down versus bottom-up control of attention in the prefrontal and posterior parietal cortices. *Science*. 2007:315:1860–1862.

Caminiti R, Carducci F, Piervincenzi C, Battaglia-Mayer A, Confalone G, Visco-Comandini F, Pantano P, Innocenti GM. Diameter, length, speed, and conduction delay of callosal axons in macaque monkeys and humans: comparing data from histology and magnetic resonance imaging diffusion tractography. *J Neurosci*. 2013:33:14501–14511.

Cavada C, Goldman-Rakic PS. Posterior parietal cortex in rhesus monkey: I. Parcellation of areas based on distinctive limbic and sensory corticocortical connections. *J Comp Neurol*. 1989a:287:393–421.

Cavada C, Goldman-Rakic PS. Posterior parietal cortex in rhesus monkey: II. Evidence for segregated corticocortical networks linking sensory and limbic areas with the frontal lobe. *J Comp Neurol*. 1989b:287:422–445.

Chafee MV, Goldman-Rakic PS. Matching patterns of activity in primate prefrontal area 8a and parietal area 7ip neurons during a spatial working memory task. *J Neurophysiol*. 1998:79:2919–2940.

Chafee MV, Goldman-Rakic P. Inactivation of parietal and prefrontal cortex reveals interdependence of neural activtity during memory-guided saccades. *J Neurophysiol*. 2000:83:1550–1566.

Constantinidis C, Steinmetz MA. Neuronal activity in posterior parietal area 7a during the delay periods of a spatial memory task. *J Neurophysiol*. 1996:76:1352–1355.

Crowe DA, Goodwin SJ, Blackman RK, Sakellaridi S, Sponheim SR, MacDonald AW 3rd, Chafee MV. Prefrontal neurons transmit signals to parietal neurons that reflect executive control of cognition. *Nat Neurosci*. 2013:16:1484–1491.

Elston GN. Pyramidal cells of the frontal lobe: all the more spinous to think with. *J Neurosci*. 2000:20RC95:91–94.

Fakhry A, Zeng T, Peng H, Ji S. Global analysis of gene expression and projection target correlations in the mouse brain. *Brain Informatics*. 2015:2:107–117.

Friedman HR, Goldman-Rakic PS. Coactivation of prefrontal cortex and inferior parietal cortex in working memory tasks revealed by 2DG functional mapping in the rhesus monkey. *J Neurosci*. 1994:14:2775–2788.

Goldman-Rakic PS. Topography of cognition: parallel distributed networks in primate association cortex. *Ann RevNeurosci*. 1988:11:137–156.

Goldman-Rakic PS. Cellular basis of working memory. *Neuron*. 1995:14:477–485.

Gonzalez-Burgos G, Miyamae T, Krimer Y, Gulchina Y, Pafundo DE, Krimer O, Bazmi H, Arion D, Enwright JF, Fish KN, et al. Distinct properties of layer 3 pyramidal neurons from prefrontal and parietal areas of the monkey neocortex. *J Neurosci*. 2019:39:7277–7290.

Hahn B, Robinson BM, Leonard CJ, Luck SJ, Gold JM. Posterior parietal cortex dysfunction is central to working memory storage and broad cognitive deficits in schizophrenia. *J Neurosci*. 2018:38:8378–8387.

Hart E, Huk AC. Recurrent circuit dynamics underlie persistent activity in the macaque frontoparietal network. *Elife*. 2020:9.

Hawrylycz MJ, Lein ES, Guillozet-Bongaarts AL, Shen EH, Ng L, Miller JA, van de Lagemaat LN, Smith KA, Ebbert A, Riley ZL, et al. An anatomically comprehensive atlas of the adult human brain transcriptome. *Nature*. 2012:489:391–399.

Hof PR, Nimchinsky EA, Morrison JH. Neurochemical phenotype of corticocortical connections in the macaque monkey: quantitative analysis of a subset of neurofilament protein-immunoreactive projection neurons in frontal, parietal, temporal, and cingulate cortices. *J Comp Neurol*. 1995:362:109–133.

Jacob SN, Nieder A. Complementary roles for primate frontal and parietal cortex in guarding working memory from distractor stimuli. *Neuron*. 2014:83:226–237.

Johnson PB, Angelucci A, Ziparo RM, Minciacchi D, Bentivoglio M, Caminiti R. Segregation and overlap of callosal and association neurons in frontal and parietal cortices of primates: a spectral and coherency analysis. *J Neurosci*. 1989:9:2313–2326.

Johnson WE, Li C, Rabinovic A. Adjusting batch effects in microarray expression data using empirical Bayes methods. *Biostatistics*. 2007:8:118–127.

Johnson MB, Kawasawa YI, Mason CE, Krsnik Z, Coppola G, Bogdanovic D, Geschwind DH, Mane SM, State MW, Sestan N. Functional and evolutionary insights into human brain development through global transcriptome analysis. *Neuron*. 2009:62:494–509.

Katsuki F, Constantinidis C. Time course of functional connectivity in primate dorsolateral prefrontal and posterior parietal cortex during working memory. *PLoS One*. 2013:8:1–12.

Klingler E, De la Rossa A, Fievre S, Devaraju K, Abe P, Jabaudon D. A Translaminar Genetic Logic for the Circuit Identity of Intracortically Projecting Neurons. *Curr Biol*. 2019:29:332, e335–339.

LaMantia AS, Rakic P. Axon overproduction and elimination in the corpus callosum of the developing rhesus monkey. *J Neurosci*. 1990:10:2156–2175.

Lanciego JL, Wouterlood FG. A half century of experimental neuroanatomical tracing. *J Chem Neuroanat*. 2011:42:157–183.

Lundqvist M, Bastos AM, Miller EK. Preservation and Changes in Oscillatory Dynamics across the Cortical Hierarchy. *J Cogn Neurosci*. 2020:32:2024–2035.

Markov NT, Ercsey-Ravasz M, Lamy C, Ribeiro-Gomes AR, Magrou L, Misery P, Giroud P, Barone P, Dehay C, Toroczkai Z, et al. The role of long-range connections on the specificity of the macaque interareal cortical network. *PNAS*. 2013:110:5187–5192.

Meissirel C, Dehay C, Berland M, Kennedy H. Segregation of callosal and association pathways during development in the visual cortex of the primate. *J Neurosci*. 1991:77:3297–3316.

Miller EK, Cohen JD. An integrative theory of prefrontal cortex function. *Annu Rev Neurosci*. 2001:24:167–202.

Miller EK, Desimone R. Parallel neuronal mechanisms for short-term memory. *Science*. 1994:263:520–522.

Miller EK, Erickson CA, Desimone R. Neural mechanisms of visual working memory in prefrontal cortex of the macaque. *J Neurosci*. 1996:16:5154–5167.

Miller EK, Lundqvist M, Bastos AM. Working memory 2.0. *Neuron*. 2018:100:463–475.

Mitchell BD, Macklis JD. Large-scale maintenance of dual projections by callosal and frontal cortical projections neurons in adult mice. *J Comp Neurol*. 2005:482:17–32.

Miyashita T, Chang HS. Neuronal correlate of pictorial short-term memory in the primate temporal cortex. *Nature*. 1988:331:68–70.

Morrison JH, Lewis DA, Campbell MJ, Huntley GW, Benson DL, Bouras C. A monoclonal antibody to non-phosphorylated neurofilament protein marks the vulnerable cortical neurons in Alzheimer's disease. *Brain Res*. 1987:416:331–336.

Petrides M, Pandya DN. Association fiber pathways to the frontal cortex from the superior temporal region in the rhesus monkey. *J Comp Neurol*. 1988:273:52–66.

Quintana J, Fuster JM, Yajeya J. Effects of cooling parietal cortex on prefrontal units in delay tasks. *Brain Res*. 1989:503:100–110.

Ritchie ME, Phipson B, Wu D, Hu Y, Law CW, Shi W, Smyth GK. limma powers differential expression analyses for RNA-sequencing and microarray studies. *Nucleic Acids Res*. 2015:43:e47.

Salazar RF, Dotson NM, Bressler SL, Gray CM. Content-specific fronto-parietal synchronization during visual working memory. *Science*. 2012:338:1097–1100.

Saleeba C, Dempsey B, Le S, Goodchild A, McMullan S. A student's guide to neural circuit tracing. *Front Neurosci*. 2019:13:897.

Schwartz ML, Goldman-Rakic PS. Single cortical neurones have axon collaterals to ipsilateral and contralateral cortex in fetal and adult primates. *Nature*. 1982:299:154–155.

Schwartz ML, Goldman-Rakic PS. Callosal and intrahemispheric connectivity of the prefrontal association cortex in rhesus monkey: relation between intraparietal and principal sulcal cortex. *J Comp Neurol*. 1984:226:403–420.

Schwartz ML, Goldman-Rakic PS. Prenatal specification of callosal connections in rhesus monkey. *J Comp Neurol*. 1991:307:144–162.

Schwartz ML, Rakic P, Goldman-Rakic PS. Early phenotype expression of cortical neurons: Evidence that a subclass of migrating neurons have callosal axons. *Proc Natl Acad Sci USA*. 1991:88:1354–1358.

Soloway AS, Pucak ML, Melchitzky DS, Lewis DA. Dendritic morphology of callosal and ipsilateral projection neurons in monkey prefrontal cortex. *Neuroscience*. 2002:109:461–471.

Sorensen SA, Bernard A, Menon V, Royall JJ, Glattfelder KJ, Desta T, Hirokawa K, Mortrud M, Miller JA, Zeng H, et al. Correlated gene expression and target specificity demonstrate excitatory projection neuron diversity. *Cereb Cortex*. 2015:25:433–449.

Suzuki M, Gottlieb J. Distinct neural mechanisms of distractor suppression in the frontal and parietal lobe. *Nat Neurosci*. 2013:16:98–104.

Tomioka R, Rockland KS. Long-distance corticocortical GABAergic neurons in the adult monkey white and gray matter. *J Comp Neurol*. 2007:505:526–538.